

Innermost stable circular orbits in Majumdar–Papapetrou dihole spacetime

Keisuke Nakashi^{1,*} and Takahisa Igata^{1,†}

¹*Department of Physics, Rikkyo University, Toshima, Tokyo 171-8501, Japan*

(Dated: June 27, 2019)

We investigate the positions of stable circular massive particle orbits in the Majumdar–Papapetrou dihole spacetime with equal mass. In terms of qualitative differences of their sequences, we classify the dihole separation into five ranges and find four critical values as the boundaries. When the separation is relatively large, the sequence on the symmetric plane bifurcates, and furthermore, they extend to each innermost stable circular orbit in the vicinity of each black hole. In a certain separation range, the sequence on the symmetric plane separates into two parts. On the basis of this phenomenon, we discuss the formation of double accretion disks with a common center. Finally, we clarify the dependence of the radii of marginally stable circular orbits and innermost stable circular orbits on the separation parameter. We find a discontinuous transition of the innermost stable circular orbit radius. We also find the separation range at which the radius of the innermost stable circular orbit can be smaller than that of the stable circular photon orbit.

I. INTRODUCTION

In 2015, the LIGO Scientific and Virgo Collaborations detected gravitational waves from a binary black hole [1, 2]. This observation established that the binary black hole systems exist in nature. So far, we have already found ten binary black hole mergers and one binary neutron star merger [3, 4], and the number of detections will increase further in the future. These discoveries strongly motivate the study of phenomena around a binary black hole system.

Actual binary black hole systems are so dynamic that the method of numerical relativity is quite useful to describe phenomena in these systems. On the other hand, it is also significant to use analytical methods for a qualitative understanding of the phenomena. However, there is no analytical expression of a binary black hole system due to their dynamical character. Therefore, we often adopt a static (or stationary) and axisymmetric dihole spacetime as a toy model. There are some dihole solutions of the Einstein equation (or the Einstein–Maxwell equation) with these symmetries, such as the Weyl spacetime [5], the Majumdar–Papapetrou spacetime [6–8], the double-Kerr spacetime [9], etc. We can learn a lot from phenomena on such a spacetime and obtain strong suggestions to binary black hole events. For example, while the formation of binary black hole shadows requires fully nonlinear simulation of numerical relativity, we can identify some specific features by using a (quasi-)static dihole spacetime [10–14].

The research of test particle motion in strong gravitational fields is significant in astrophysics as well as in gravitational theories. Even in binary black hole systems, it is still one of the most fundamental problems. Indeed, the formation of the binary black hole shadow mentioned above is the problem of the dynamics of massless particles. On the other hand, the dynamics of massive particles in a binary black hole system has been discussed in the contexts of gravitational wave radiation induced by a third body effect [15–18] and the formation of multiple accretion disks [19, 20]. In these phenomena, the sequence of stable circular orbits is crucial, and in particular, the innermost stable circular orbit (ISCO) plays a key role because it is expected to be the inner edge of an accretion disk [21], and also an inspiralling compact binary transits into the merging phase there [22, 23].

Under these circumstances, the purpose of this paper is to clarify the characteristics of stable circular orbits in a binary black hole system. In particular, it is meaningful to study how marginally stable circular orbits (or innermost stable circular orbits) of a binary black hole system changes compared to those of a single black hole. To achieve this, we consider stable circular orbits around the axis of symmetry of the dihole in the equal mass Majumdar–Papapetrou (MP) spacetime, which is an exact solution of the Einstein–Maxwell equation and consists of two extremal Reissner–Nordström black holes. Once we fix the mass scale of the dihole, it depends only on one parameter, the dihole separation. We expect that the stable circular orbits exhibit nontrivial appearance when the separation between two black holes changes. Indeed, in some previous works, several properties of stable circular orbits in the MP dihole spacetime were reported: marginally stable circular orbits of massive particles are not unique [24] and the stable circular photon orbit appears inside the unstable circular photon orbit [25]. In this paper, we analyze the dependence of the sequence of stable circular orbits on the separation parameter in the whole

*Electronic address: nakashi@rikkyo.ac.jp

†Electronic address: igata@rikkyo.ac.jp

spacetime. As a result of our analysis, the parameter range is divided into five, at each boundary of which the behavior of stable circular orbits drastically changes. Then we find the appearance of marginally stable circular orbits, ISCOs, and the stable/unstable circular photon orbit. Note that the marginally stable circular orbit is unique in the Schwarzschild/Reissner–Nordström/(charged) Kerr spacetime but not in the MP dihole spacetime. Therefore, the ISCO is the marginally stable circular orbit with the smallest radius. Finally, we find that the position of the ISCO transits discontinuously at a certain value of the separation and the radius of the ISCO is smaller than the stable circular photon orbit for a specific separation.

This paper is organized as follows. In Sec. II, we derive the conditions of stability for circular orbits of a massive particle in the MP dihole spacetime with equal mass. These conditions are given in terms of a 2D effective potential and its Hessian. In Sec. III, we explore the dependence of the sequence of stable circular orbits on the separation between the dihole. Dividing the range of the separation parameter into five parts, we clarify the transitions of marginally stable circular orbits and the innermost stable circular orbit. Furthermore, by analyzing qualitative changes of the sequence of stable circular orbits, we find some critical values of the separation parameter analytically. Section IV is devoted to a summary and discussions. We use units in which $G = 1$ and $c = 1$.

II. STABILITY CONDITIONS OF CIRCULAR ORBITS IN THE MAJUMDAR–PAPAPETROU DIHOLE SPACETIME WITH EQUAL MASS

The metric and the gauge field of the Majumdar–Papapetrou (MP) dihole spacetime in isotropic coordinates are given by

$$g_{\mu\nu}dx^\mu dx^\nu = -\frac{dt^2}{U^2} + U^2 (d\rho^2 + \rho^2 d\phi^2 + dz^2), \quad (1)$$

$$A_\mu dx^\mu = U^{-1} dt, \quad (2)$$

$$U(\rho, z) = 1 + \frac{M_+}{\sqrt{\rho^2 + (z-a)^2}} + \frac{M_-}{\sqrt{\rho^2 + (z+a)^2}}, \quad (3)$$

where M_\pm are masses of two extremal Reissner–Nordström black holes located at $z = \pm a$ ($a \geq 0$). Note that we choose cylindrical coordinates on the spatial geometry, $x = \rho \cos \phi$ and $y = \rho \sin \phi$, where x, y are the Cartesian coordinates.

The Lagrangian \mathcal{L} of a freely falling test particle is defined by

$$\mathcal{L} = \frac{1}{2} g_{\mu\nu} \dot{x}^\mu \dot{x}^\nu = \frac{1}{2} \left[-\frac{\dot{t}^2}{U^2} + U^2 (\dot{\rho}^2 + \rho^2 \dot{\phi}^2 + \dot{z}^2) \right], \quad (4)$$

where the dot denotes derivative with respect to an affine parameter. Since the spacetime is static and axisymmetric, the Lagrangian does not depend on the coordinates t and ϕ explicitly. Thus, there are two constants of motion

$$E = \frac{\dot{t}}{U^2}, \quad L = \rho^2 U^2 \dot{\phi}, \quad (5)$$

where we may assume that $E > 0$. These quantities correspond to energy and angular momentum, respectively. Without loss of generality, we assume that the worldline is parametrized so that $g_{\mu\nu} \dot{x}^\mu \dot{x}^\nu = -\kappa$, where $\kappa = 1$ for timelike particles and $\kappa = 0$ for null particles. From this normalization and Eqs. (5), we introduce the effective potential $V(\rho, z)$ for the motion in ρ - z plane

$$\dot{\rho}^2 + \dot{z}^2 + V = E^2, \quad (6)$$

$$V(\rho, z; L^2) = \frac{L^2}{\rho^2 U^4} + \frac{\kappa}{U^2}. \quad (7)$$

We consider circular orbits with constant ρ and z for timelike particles. Particles in circular orbits must satisfy the following conditions: (a) $\dot{\rho} = \dot{z} = 0$, (b) $\ddot{\rho} = \ddot{z} = 0$. Condition (a) together with the normalization (6) leads to

$$V = E^2. \quad (8)$$

Conditions (8), (a), and (b) together with the equations of motion for z and ρ imply

$$V_z = 0, \quad (9)$$

$$V_\rho = 0, \quad (10)$$

where $V_i = \partial_i V$ ($i = z, \rho$). Hence the circular orbits are realized at stationary points of V where the values of V are positive.

We can rewrite Eqs. (8), (9), and (10) by using the explicit form (7) as

$$U_z = 0, \quad (11)$$

$$L^2 = L_0^2(\rho, z) := -\frac{\rho^3 U^2 U_\rho}{U + 2\rho U_\rho}, \quad (12)$$

$$E^2 = E_0^2(\rho, z) := V(\rho, z; L_0^2), \quad (13)$$

where L_0^2 must be non-negative value in the physical branch. Note that, if $L_0^2 \geq 0$ holds, then V is necessarily positive. Finally, we find that a particle moves in a circular orbit with constant ρ and z if and only if the conditions $U_z = 0$, $L^2 = L_0^2 \geq 0$, and $E^2 = E_0^2$ are satisfied.

We also consider the stability of circular orbits. From the standard linear stability analysis of circular orbits, we find that a circular orbit is stable if and only if the orbit exists at a local minimum point of V . We call such a circular orbit a stable circular orbit. On the other hand, a circular orbit is unstable if and only if the orbit exists at a local maximum point of V or a saddle point of V . We call such a circular orbit an unstable circular orbit. Here we introduce the Hessian of V and the trace of $V_{ij} = \partial_i \partial_j V$

$$h(\rho, z; L^2) = \det V_{ij}, \quad (14)$$

$$k(\rho, z; L^2) = \text{Tr} V_{ij}. \quad (15)$$

In terms of these quantities, we can summarize the stability of circular motions as follows:

- (i) A circular orbit is stable $\iff h > 0$ and $k > 0$ at a stationary point of V ;
- (ii) A circular orbit is unstable $\iff (h > 0$ and $k < 0)$ or $h < 0$ at a stationary point of V .

When a sequence of stable circular orbits switches to a sequence of unstable circular orbits at a radius, we call the circular orbit at the radius a marginally stable circular orbit, where V has an inflection point (i.e., $h = 0$). In particular, we call the marginally stable circular orbit with the smallest value of the radial coordinate ρ the innermost stable circular orbit.

In the remainder of this paper, we investigate circular orbits in the MP dihole spacetime with equal mass $M_+ = M_-$. We use units in which $M_\pm = 1$ in what follows. In this case, Eq. (11) reduces to

$$z \left[\rho^6 - 3(a^2 - z^2)^2 \rho^2 - 2(a^2 + z^2)(a^2 - z^2)^2 \right] = 0. \quad (16)$$

This equation means that U_z always vanishes on the symmetric plane $z = 0$. Focusing on the case where the inside of the square bracket vanishes, we find another real root of Eq. (11)

$$\rho_0^2 = 2(a^2 - z^2) \cos \left[\frac{1}{3} \arccos \frac{a^2 + z^2}{a^2 - z^2} \right]. \quad (17)$$

Hence we obtain two curves $z = 0$ and $\rho = \rho_0(z)$ in ρ - z plane, where U_z vanishes. Note that these curves intersect each other at $(\rho, z) = (\sqrt{2}a, 0)$. To discuss the stability of circular orbits, we introduce the Hessian h and the trace k evaluated at $L^2 = L_0^2$

$$h_0(\rho, z) = h(\rho, z; L_0^2)|_{U_z=0}, \quad (18)$$

$$k_0(\rho, z) = k(\rho, z; L_0^2)|_{U_z=0}, \quad (19)$$

where the restriction $U_z = 0$ means that the terms directly proportional to U_z have been removed from the right-hand sides. Using h_0 and k_0 , we specify the region where the remaining conditions for stable circular orbits hold

$$D = \{(\rho, z) \mid h_0 > 0, k_0 > 0, L_0^2 > 0\}. \quad (20)$$

Hence, stable circular orbits in the MP dihole spacetime with equal mass exist on the curves $z = 0$ or $\rho = \rho_0$ included in the region D in ρ - z plane.

It is convenient to obtain the expressions L_0 , E_0 , and h_0 evaluated at the symmetric plane $z = 0$. To derive them in simpler forms, we use a new coordinate R defined by

$$R(\rho) = \sqrt{\rho^2 + a^2}, \quad (21)$$

where $R \geq a$, which follows from $\rho \geq 0$. In terms of R , we derive angular momentum and energy for a circular orbit on $z = 0$, respectively,

$$L_0(\rho, 0) = \frac{\sqrt{2}(R+2)(R^2 - a^2)}{R\sqrt{f}}, \quad (22)$$

$$E_0(\rho, 0) = \frac{R\sqrt{R^3 + 2a^2}}{(R+2)\sqrt{f}}, \quad (23)$$

where, without loss of generality, we have chosen the branch $L_0 \geq 0$, and

$$f(R) = R^3 - 2R^2 + 4a^2. \quad (24)$$

Note that these quantities diverge if f vanishes. Furthermore, in the range $f < 0$, there is no circular orbit (see Sec. III F for details). In addition, the derivatives of $L_0(\rho, 0)$ and $E_0(\rho, 0)$ with respect to R are given by, respectively,

$$\frac{dL_0(\rho, 0)}{dR} = \frac{g}{\sqrt{2}R^2 f^{3/2}}, \quad (25)$$

$$\frac{dE_0(\rho, 0)}{dR} = \frac{g}{(R+2)^2 \sqrt{R^3 + 2a^2} f^{3/2}}, \quad (26)$$

where

$$g(R) = R^6 - 6R^5 + 3a^2 R^4 + 22a^2 R^3 + 16a^4. \quad (27)$$

These results mean that the monotonicity of angular momentum and energy for a circular orbit switches at the points where $g = 0$. We find that, at least in the region far enough from the center $R \gg a$, the angular momentum $L_0(\rho, 0)$ and the energy $E_0(\rho, 0)$ are real positive values and monotonically increasing with R . We also derive h_0 evaluated at $z = 0$

$$h_0(\rho, 0) = \frac{16(R^2 - 3a^2)g}{R^2(R+2)^6 f^2}. \quad (28)$$

If f vanishes, this quantity diverges, which is similar to the behaviors seen in $L_0(\rho, 0)$ and $E_0(\rho, 0)$. On the other hand, the Hessian $h_0(\rho, 0)$ vanishes at $R = \sqrt{3}a$ (i.e., $\rho = \sqrt{2}a$), where $z = 0$ and $\rho = \rho_0$ intersect each other. In addition, $h_0(\rho, 0)$ also vanishes for $g = 0$, which is similar to the behavior seen in Eqs. (25) and (26). This fact implies that the monotonicity of angular momentum and energy for a circular orbit switches at zeros of $h_0(\rho, 0)$. Taking into account $h_0(\rho, 0) > 0$ for $R \gg a$, we find that angular momentum and energy monotonically increase with R on the sequence of stable circular orbits and monotonically decrease with R on the sequence of unstable circular orbits.

III. DEPENDENCE OF THE SEQUENCE OF STABLE CIRCULAR ORBITS ON THE SEPARATION

We discuss the dependence of the positions of stable circular orbits on the separation parameter a . Using the functions defined in the previous section, we plot the sequence of stable circular orbits as illustrated in Figs. 1. On the basis of these plots, dividing the range of a into five parts, we clarify the behavior of stable circular orbits for each range of a in the following subsections. Furthermore, we find the four critical values of a characterized by the behaviors of the sequence of stable circular orbits and the angular momentum of a circular orbit.

A. $a > 1.401 \dots$

We focus on stable circular orbits in the case where the separation between the dihole is large enough (i.e., $a \gg 1$). Figure 1(a) shows a typical shape of the sequence of stable circular orbits for a large value of a . As seen from the figure, stable circular orbits exist on the line $z = 0$ in the range $\rho \in (\sqrt{2}a, \infty)$. The end point $(\rho, z) = (\sqrt{2}a, 0)$ is a marginally stable circular orbit because the sequence switches to that of unstable circular orbits at this point, where $h_0 = 0$. In addition, at this point the sequence of stable circular orbits bifurcates into the curve $\rho = \rho_0$, where ρ_0 is defined by Eq. (17). Finally it terminates near each black hole, which also correspond to marginally stable circular orbits, especially the ISCOs.

Even in the sequence on $\rho = \rho_0$, the energy and the angular momentum of stable circular orbits monotonically decrease as the radius decreases up to the ISCOs. Note that, when a is large enough, a particle moving near each black hole feels gravity of a single black hole. Indeed, in the limit as $a \rightarrow \infty$, the ISCO radius measured by ρ approaches 3, which coincides with the ISCO radius of the single extremal Reissner–Nordström black hole spacetime (see Appendix B).

As the value of a decreases from a large value, the ISCOs approach the intersection of $z = 0$ line and $\rho = \rho_0$ line. When the value of a reaches $1.401\dots$, the three marginally stable circular orbits merge at a point on $z = 0$ [see Fig. 1(b)]. As a result, the sequence of stable circular orbits only appears on the line $z = 0$.

B. $a = a_0 = 1.401\dots$

We find the critical value $a = a_0$ at which the three marginally stable circular orbits degenerate [see Fig. 1(b)]. We expand ρ_0 in Eq. (17) around $z = 0$ up to $O(z^2)$,

$$\rho_0 = \sqrt{2}a - \frac{7}{9\sqrt{2}a}z^2 + O(z^4). \quad (29)$$

Substituting this expression into h_0 , we expand it around $z = 0$ again,

$$h_0(\rho_0, z) = \frac{768(54a^2 - 33\sqrt{3}a - 26)}{a^2(9a - 2\sqrt{3})^2(3a + 2\sqrt{3})^6}z^2 + O(z^4). \quad (30)$$

As already discussed above, these results imply that there exists a marginally stable circular orbit at the point $(\rho, z) = (\sqrt{2}a, 0)$. Furthermore, since the condition of the multiple root is $d^2h_0(\rho_0, z)/dz^2 = O(z^2)$, i.e., $54a^2 - 33\sqrt{3}a - 26 = 0$, we obtain the critical value a_0 as

$$a_0 = \frac{11 + \sqrt{329}}{12\sqrt{3}} = 1.401\dots \quad (31)$$

Thus, in the case $a = a_0$, we find stable circular orbits on $z = 0$ plane in the range $\rho \in (\sqrt{2}a_0, \infty)$ and the ISCO at $(\rho, z) = (\sqrt{2}a_0, 0)$.

C. $a_0 > a > 0.9713\dots$

If we make a smaller than a_0 , the sequence of stable circular orbits still appears only on $z = 0$ plane in the range $\rho \in (\sqrt{2}a, \infty)$ [see Fig. 1(c)], so that it is sufficient to analyze circular orbits on it. The end point $(\rho, z) = (\sqrt{2}a, 0)$ corresponds to the unique marginally stable circular orbit, especially the ISCO. When the value of a reaches $0.9713\dots$, the region D becomes marginally connected at the intersection point of the lines $z = 0$ and $h_0 = 0$ [see Fig. 1(d)]. This intersection point is not a marginally stable circular orbit because the sequence of stable circular orbits does not switch to that of unstable circular orbits here. As a result, there exists the unique marginally stable circular orbit in the range $a_0 \geq a \geq 0.9713\dots$.

D. $a = a_* = 0.9713\dots$

We seek the exact critical value $a = a_*$ at which the region D is marginally connected at the intersection point of the lines $z = 0$ and $h_0 = 0$ [see Fig. 1(d)]. In other words, the function h_0 has a saddle point at this point. We use this condition to derive a_* in what follows. From the explicit form of $h_0(\rho, 0)$ given in Eq. (28), we find that the condition $h_0(\rho, 0) = 0$ holds at $(R, z) = (\sqrt{3}a, 0)$, but the Hessian h_0 does not have a stationary point there. Therefore we focus on the other branch

$$g = 0, \quad (32)$$

where g is defined by Eq. (27). A point satisfying this equation can be a stationary point of h_0 if $dh_0(\rho, 0)/dR = 0$, which reduces to

$$R^3 - 5R^2 + 2a^2R + 11a^2 = 0, \quad (33)$$

where we have used Eq. (32). Solving Eqs. (32) and (33) for a and R simultaneously, then we obtain the solutions

$$a_* = \frac{50(7 + \sqrt{129})}{(13 + \sqrt{129})\sqrt{710 + 70\sqrt{129}}} = 0.9713\dots, \quad (34)$$

$$R_* = \frac{-19 + 3\sqrt{129}}{4} = 3.768\dots. \quad (35)$$

The value of ρ corresponding to these solutions is given by

$$\rho_* = \frac{5}{512}(20291 - 1667\sqrt{129}) = 3.641\dots. \quad (36)$$

The inverse of a_* coincides with the critical values M_* mentioned in Ref. [24]. Note that the linear stability of a circularly orbiting particle at $(\rho, z) = (\rho_*, 0)$ is undetermined, but the analysis of the allowed region of the particle motion shows it nonlinearly stable.

E. $a_* > a > 0.5433\dots$

If we make a smaller than a_* , the region D is separated into two regions [see Fig. 1(e)], and then two sequences of stable circular orbits appear on the line $z = 0$. The outer sequence appears from infinity to a marginally stable circular orbit, while the inner sequence appears between another marginally stable circular orbit and the ISCO. Therefore, three marginally stable circular orbits appear in total as the boundaries of these sequences. Their radii except for the ISCO radius are given as real roots for Eq. (32), and the ISCO radius is $\rho = \sqrt{2}a$ in particular.

As the value of a gradually decreases, the two sequences tend to separate from each other. In addition, the energy at the marginally stable circular orbit next to the ISCO increases. Remarkably, it reaches the energy level of a rest particle at infinity (i.e., $E = 1$) at $a = 0.7567\dots$. Hence, for $a \leq 0.7567\dots$, stable circular orbits with $E_0 \geq 1$ exist until the inner sequence disappears. Note that we do not observe such a phenomenon in the Kerr spacetime. Since circular orbits with $E_0 \leq 1$ occur more naturally, the sequence with $E_0 > 1$ does not contribute to phenomena such as accretion disk formation around the dihole.

When the value of a reaches $0.5433\dots$, the marginally stable circular orbit next to the ISCO is no longer a circular orbit because infinitely large angular momentum and energy are required to keep it a circular orbit [see Fig. 1(f)]. In the following subsection, we find the critical value of a from the behavior of L_0^2 .

F. $a = a_\infty = 0.5433\dots$

As mentioned in the previous subsection, one of the three marginally stable circular orbits located next to the ISCO disappears in the limit as $a \searrow 0.5433\dots$. If a timelike particle circularly orbited at this limiting radius for $a = 0.5433\dots$, the angular momentum L_0^2 would diverge. Therefore, to find the exact critical value a_∞ of a , we analyze the behavior of $L_0^2(\rho, 0)$, which is given by Eq. (22). Notice that this expression and Eq. (28) diverge if the following condition is satisfied:

$$f = 0. \quad (37)$$

It is worth pointing out that this condition is equivalent to that of the existence of circular photon orbits (see Appendix B). Since $f(R)$ has a local minimum at $R = 4/3$ and its extreme value takes the form $f(4/3) = 4(a^2 - 8/27)$, we find that the divergence of L_0^2 appears only at $\rho = \rho_\infty$ for $a = a_\infty$, where

$$a_\infty = \frac{2\sqrt{6}}{9} = 0.5433\dots, \quad (38)$$

$$\rho_\infty = \frac{2\sqrt{30}}{9} = 1.217\dots, \quad (39)$$

where ρ_∞ corresponds to $R = 4/3$. At $a = a_\infty$, hence the inner sequence of stable circular orbits on $z = 0$ plane exist in the range $\rho \in (\sqrt{2}a_\infty, \rho_\infty)$. The inverse of a_∞ coincides with \bar{M} mentioned in Ref. [24].

For $a > a_\infty$, the angular momentum $L_0^2(\rho, 0)$ is positive and finite everywhere. This means that there exist stable/unstable circular orbits with arbitrary radii on $z = 0$ plane. On the other hand, for $a \leq a_\infty$, there exists no circular orbit of a massive particle on $z = 0$ plane in the range $\rho_{\text{ps}} \leq \rho \leq \rho_{\text{pu}}$ because L_0^2 can be negative or infinitely large there, where ρ_{ps} and ρ_{pu} are defined in Eqs. (B4) and (B5).

G. $a_\infty > a > 0.3849\dots$

If we make a smaller than a_∞ , there still exist the two sequences of stable circular orbits on $z = 0$ plane [see Fig. 1(g)]. The outer sequence exists from infinity to a marginally stable circular orbit. The inner sequence exists in the range $\rho \in (\sqrt{2}a, \rho_{\text{ps}})$, where $\rho = \sqrt{2}a$ is the ISCO radius and $\rho = \rho_{\text{ps}}$ is the radius of the stable circular photon orbit, defined by Eq. (B5) in Appendix B. The ISCO radius is smaller than the radius of the stable circular photon orbit. Note that L_0^2 diverges in the limit as $\rho \rightarrow \rho_{\text{ps}}$ on the inner sequence, which is consistent with the appearance of the stable circular photon orbit.

As the value of a approaches $0.3849\dots$, the value ρ_{ps} approaches $\sqrt{2}a$. When $a = 0.3849\dots$, the inner sequence disappears [see Fig. 1(h)].

H. $a = a_c = 0.3849\dots$

We seek the exact critical value of $a = 0.3849\dots$ at which the inner sequence of stable circular orbits just disappears. The value of L_0^2 at $(\rho, z) = (\sqrt{2}a, 0)$ is given by

$$L_0^2(\sqrt{2}a, 0) = \frac{8(a + 3a_c)^2}{3\sqrt{3}(a - a_c)}, \quad (40)$$

where

$$a_c = \frac{2\sqrt{3}}{9} = 0.3849\dots \quad (41)$$

This result together with Eq. (28) means that, even if a arbitrarily approaches to a_c from above, the point $(\rho, z) = (\sqrt{2}a, 0)$ is necessarily a marginally stable circular orbit. If $a = a_c$, then L_0^2 at $(\rho, z) = (\sqrt{2}a_c, 0)$ diverges, so that the inner sequence of stable circular orbits disappears. Consequently, we can identify a_c with the numerical critical value $a = 0.3849\dots$. Thus the location of the ISCO changes discontinuously at $a = a_c$. Note that, however, the circular photon orbit exists there.

I. $a_c > a \geq 0$

If we make a smaller than a_c , the single sequence of stable circular orbits appears on $z = 0$ plane from infinity to the ISCO. As the value of a approaches 0, the ISCO radius monotonically increases. For $a = 0$, the MP dihole becomes the single extremal Reissner–Nordström black hole with mass equal to 2 in our units. Then the sequence of stable circular orbits exists from infinity to the ISCO radius equal to three times its mass (see Appendix A). Therefore, we find the ISCO at $\rho = 6$ as shown in Fig. 1(i). Note that $z = 0$ plane at $a = 0$ is no longer special because spherical symmetry is restored.

IV. SUMMARY AND DISCUSSIONS

We have investigated stable circular orbits in the Majumdar–Papapetrou dihole spacetime with equal unit mass for various values of the dihole separation. We have divided the separation parameter a into five ranges based on qualitative differences of the sequence of stable circular orbits and simultaneously have determined the four critical values as the boundaries of the ranges: a_0, a_*, a_∞ and a_c . For $a > a_0 = 1.401\dots$, the sequence of stable circular orbits exists on the symmetric plane and further bifurcates and extends towards each black hole. This phenomenon is a clear sign to recognize a dihole. On the other hand, for $0 \leq a \leq a_0$, stable circular orbits lie only on the symmetric plane. In both ranges $a_0 \geq a > a_* = 0.9713\dots$ and $0 \leq a \leq a_c = 0.3849\dots$, stable circular orbits form a continuous single sequence, while in the range $a_c < a \leq a_*$, stable circular orbits form two separated sequences.

With the transition of the sequence of stable circular orbits, the numbers of marginally stable circular orbits changes. We have summarized them in Table I. The number of the marginally stable circular orbits increases due to the bifurcation or the separation of the sequence. The radii of marginally stable circular orbits and the ISCOs are plotted as a function of a in Fig. 2. The ISCO radius, shown by red lines, can be smaller than the ISCO radius in the single extremal Reissner–Nordström black hole spacetime. The location of the ISCO changes discontinuously at $a = a_c$.

separation	MSCOs	$n(\text{MSCOs})$	ISCOs	$n(\text{ISCOs})$
A. $a > a_0 = 1.401 \dots$	(ρ_0, z) where $h_0(\rho_0, z) = 0, z \leq a$	3	(ρ_0, z) where $h_0(\rho_0, z) = 0, z \neq 0$	2
B. $a = a_0$	$(\sqrt{2}a_0, 0)$	1	$(\sqrt{2}a_0, 0)$	1
C. $a_0 > a > a_* = 0.9713 \dots$	$(\sqrt{2}a, 0)$	1	$(\sqrt{2}a, 0)$	1
D. $a = a_*$	$(\sqrt{2}a_*, 0)$	1	$(\sqrt{2}a_*, 0)$	1
E. $a_* > a > a_\infty = 0.5433 \dots$	$(\rho, 0)$ where $h_0(\rho, 0) = 0$	3	$(\sqrt{2}a, 0)$	1
F. $a = a_\infty$	$(\rho, 0)$ where $h_0(\rho, 0) = 0, 0 \leq L_0^2 < \infty$	2	$(\sqrt{2}a_\infty, 0)$	1
G. $a_\infty > a > a_c = 0.3849 \dots$	$(\rho, 0)$ where $h_0(\rho, 0) = 0, 0 \leq L_0^2 < \infty$	2	$(\sqrt{2}a, 0)$	1
H. $a = a_c$	$(\rho, 0)$ where $h_0(\rho, 0) = 0$	1	$(\rho, 0)$ where $h_0(\rho, 0) = 0$	1
I. $a_c > a \geq 0$	$(\rho, 0)$ where $h_0(\rho, 0) = 0$	1	$(\rho, 0)$ where $h_0(\rho, 0) = 0$	1

TABLE I: Positions in ρ - z plane and the numbers of the marginally stable circular orbits (MSCOs) and the innermost stable circular orbits (ISCOs) for each range of the separation parameter a . The item $n(\text{MSCOs})$ indicates the number of the marginally stable circular orbits, and the item $n(\text{ISCOs})$ indicates the number of the innermost stable circular orbits.

For an equal mass MP dihole with arbitrary separation, we have found stable circular orbits far from the dihole on the symmetric plane. These orbits balance by Newtonian gravitational force and centrifugal force. Near the dihole, however, stable circular orbits may balance by other mechanisms. As in the case of a familiar Schwarzschild black hole, a particle in the vicinity of the horizon feels the high-order relativistic effect. On the other hand, since there is no horizon on the symmetric plane of this dihole spacetime, the centrifugal barrier of a particle inevitably diverges at the center. As a result, a radial stable equilibrium point appears by balancing the relativistic higher-order gravitational force and centrifugal force. Furthermore, if this point is also in a region bounded in the vertical direction, a stable circular orbit occurs. This mechanics is similar to that of the appearance of stable circular orbits near the 5D black ring [26, 27]. This suggests that the phenomenon occurs universally in the spacetime where there is no horizon at the center of the system.

We briefly mention unstable circular orbits for massive particles. For an arbitrary value of $a > 0$, there exists the sequence of unstable circular orbits on the symmetric plane in the range $\rho < \sqrt{2}a$, which are radially stable but vertically unstable. The sequence further appears between the pair of marginally stable circular orbits on the symmetric plane for $a_\infty < a < a_*$ [see Fig. 1(e)], while it appears between the outermost marginally stable circular orbit and the unstable circular photon orbit for $0 \leq a \leq a_\infty$ [see Figs. 1(f)–1(i)]. In addition, we also find unstable circular orbits on $\rho = \rho_0$ for $a > a_c$. They appear between the ISCO(s) and the unstable circular photon orbits. On these sequences, the energy and the angular momentum are monotonically increases as the radius decreases.

It is worthwhile to remark on characteristic accretion disk formation on the symmetric plane. The two sequences of stable circular orbits for $a_c < a < a_*$ suggest the formation of double accretion disks with a common center. In general, it is natural for a particle in an accretion disk to fall from outside to inside while losing their energy and angular momentum. If a particle reaches the inner edge of the outer disk and loses further energy and angular momentum, it transits into a stable circular orbit in the inner disk, which has lower energy and angular momentum levels than those of the outer disk. Taking into account this mechanism, we can obtain a more restricted parameter range $a_* > a > 0.5238 \dots$ from the condition that the energy and the angular momentum levels at the inner edge of the inner disk become smaller than those at the inner edge of the outer disk. Therefore, we can conclude that the formation of double accretion disks occurs in this parameter range.

Though we have considered the MP dihole spacetime with equal mass in the present paper, the methods in the discussions above are applicable to the MP dihole spacetime with different mass. Since the MP dihole spacetime is a toy model of a realistic binary system, we need to take into account the dynamical effect for further understanding of the binary system in future work. There are some previous works taking into account the dynamical effect of the binary in the MP dihole spacetime [28, 29]. These works may help us to analyze the dynamical features of the sequence of stable circular orbits in the binary system.

Acknowledgments

The authors thank N. Asaka, T. Harada, T. Houri, D. Ida, H. Ishihara, T. Kobayashi, Y. Koga, T. Kokubu, S. Noda, K. Ogasawara, H. Saida, and R. Takahashi for their helpful discussions and useful comments. This work was supported by the MEXT-Supported Program for the Strategic Research Foundation at Private Universities, 2014–

2017 (S1411024), JSPS KAKENHI Grant No. JP19K14715 (T.I.) and Rikkyo University Special Fund for Research (K.N.).

Appendix A: Circular orbits in the extremal Reissner–Nordström black hole

We review circular orbits in the extremal Reissner–Nordström black hole spacetime. The metric in the isotropic coordinates is given by

$$g_{\mu\nu} dx^\mu dx^\nu = - \left(1 + \frac{M}{\rho}\right)^{-2} dt^2 + \left(1 + \frac{M}{\rho}\right)^2 [d\rho^2 + \rho^2(d\theta^2 + \sin^2\theta d\phi^2)], \quad (\text{A1})$$

where M is the mass of the black hole. The horizon is located at $\rho = 0$. The standard form of the metric in the Schwarzschild coordinates is recovered by the transformation $r = \rho + M$. We consider a freely falling particle in a circular orbit on the equatorial plane ($\theta = \pi/2$). Using the same procedure as in Sec. II, we obtain the radial equation

$$\dot{\rho}^2 + V = E^2, \quad (\text{A2})$$

$$V = \frac{L^2}{\rho^2} \left(1 + \frac{M}{\rho}\right)^{-4} + \kappa \left(1 + \frac{M}{\rho}\right)^{-2}, \quad (\text{A3})$$

where the dot denotes derivative with respect to an affine parameter, $E = -(1 + M/\rho)^{-2} \dot{t}$ is conserved energy, $L = (\rho + M)^2 \dot{\phi}$ is conserved angular momentum, $\kappa = 1$ for massive particles, and $\kappa = 0$ for massless particles. Circular orbits are given by the simultaneous solutions of $V = E^2$ and $dV/d\rho = 0$. The second equation for massless particles (i.e., $\kappa = 0$) has a root

$$\rho = M. \quad (\text{A4})$$

This is the radius of the circular photon orbit. In the Schwarzschild radial coordinate, the radius corresponds to $r = 2M$. There is the other root $\rho = 0$ but this is not a circular orbit. On the other hand, the equation $dV/d\rho = 0$ for massive particles (i.e., $\kappa = 1$) has the roots

$$\rho_{\pm} = \frac{L^2 - 2M^2 \pm \sqrt{L^2(L^2 - 8M^2)}}{2M}. \quad (\text{A5})$$

Note that the larger root ρ_+ is a local minimum point of V , while the smaller root ρ_- is a local maximum point of V . Thus, stable circular orbits exist at $\rho = \rho_+$, and unstable circular orbits exist at $\rho = \rho_-$. In the case $L^2 = 8M^2$, the pair of circular orbit radii coincides with each other, and then the radius takes the value

$$\rho = 3M. \quad (\text{A6})$$

This is the minimum radius of stable circular orbits and is known as the innermost stable circular orbit. In the Schwarzschild radial coordinate, the radius of the innermost stable circular orbit corresponds to $r = 4M$.

Appendix B: Circular photon orbits in the equal mass Majumdar–Papapetrou dihole spacetime

We review circular photon orbits in the MP dihole spacetime with equal unit mass $M_{\pm} = 1$. The effective potential for null particles is given by Eq. (7) with $\kappa = 0$. As is the case with timelike particles, the condition $V_z = 0$ is equivalent to $U_z = 0$ and has solutions $\rho = \rho_0$ and $z = 0$. We focus on circular photon orbits on $\rho = \rho_0$. To investigate their positions, we solve Eq. (16) again for z and find real roots $z_0(\rho)$. The line $z = z_0$ corresponds to the line $\rho = \rho_0$. We consider the condition $V_{\rho} = 0$ on $z = z_0$:

$$V_{\rho}(\rho, z_0(\rho)) = 0. \quad (\text{B1})$$

The real solutions of this equation express the radii of the unstable circular photon orbits. They only exist for $a \geq a_c$ but not for $a < a_c$. The dependence of the radii of circular photon orbits on the separation parameter a is shown in Fig. 2 by orange dashed lines. In the limit as $a \rightarrow \infty$, the circular photon orbit radius measured by ρ approaches 1, which coincides with that of the single Reissner–Nordström black hole spacetime.

Next we focus on circular photon orbits on $z = 0$ plane. The condition $V_\rho = 0$ leads to

$$(\rho^2 + a^2)^{3/2} = 2(\rho^2 - a^2). \quad (\text{B2})$$

This equation has real roots only for $\rho > a$. We can rewrite Eq. (B2)

$$f = 0, \quad (\text{B3})$$

where f is defined by Eq. (24). In the range $\rho > a$, the roots of this cubic equation for ρ^2 are given by

$$\rho_{\text{pu}}^2 = \frac{4 - 3a^2}{3} + \frac{8}{3}\sqrt{1 - 3a^2} \cos \left[\frac{1}{3} \arccos \frac{27a^4 - 36a^2 + 8}{8(1 - 3a^2)^{3/2}} \right], \quad (\text{B4})$$

$$\rho_{\text{ps}}^2 = \frac{4 - 3a^2}{3} + \frac{8}{3}\sqrt{1 - 3a^2} \cos \left[\frac{4\pi}{3} + \frac{1}{3} \arccos \frac{27a^4 - 36a^2 + 8}{8(1 - 3a^2)^{3/2}} \right]. \quad (\text{B5})$$

Note that ρ_{pu} and ρ_{ps} correspond to the unstable circular photon orbit and the stable one, respectively (see Fig. 2). These roots are real only for $a \leq a_\infty$, which is found from the discriminant of Eq. (B3). Hence, for $a > a_\infty$, there exist unstable circular photon orbits only on $\rho = \rho_0$ line [see Figs. 1(a)–1(e)]. When $a = a_\infty$, an additional circular photon orbit appears at $(\rho, z) = (\rho_\infty, 0)$ [see Fig. 1(f)], where ρ_∞ is given by Eq. (39). The condition for the existence of the multiple root $\rho_{\text{pu}} = \rho_{\text{ps}}$ also leads to the values of a_∞ and ρ_∞ . For $a_c < a < a_\infty$, unstable circular photon orbits exist on $\rho = \rho_0$ and at $(\rho, z) = (\rho_{\text{pu}}, 0)$, and stable circular photon orbits exist at $(\rho, z) = (\rho_{\text{ps}}, 0)$ [see Fig. 1(g)]. When $a = a_c$, three circular photon orbits degenerate at $(\rho, z) = (\sqrt{2}a_c, 0)$ [see Fig. 1(h)]. For $a < a_c$, there is no stable circular photon orbit but there are two unstable circular photon orbits on $z = 0$. The outer one is radially unstable but vertically stable, while the inner one is radially stable but vertically unstable (see also Ref. [30]). For $a = 0$, we obtain $\rho_{\text{pu}} = 2$ and $\rho_{\text{ps}} = 0$, which coincide with the radius of the unstable circular photon orbit and the horizon radius of the single extremal Reissner–Nordström black hole with mass 2, respectively (see Appendix A).

-
- [1] B. P. Abbott *et al.* (LIGO Scientific and Virgo Collaborations), Observation of Gravitational Waves from a Binary Black Hole Merger, *Phys. Rev. Lett.* **116**, 061102 (2016) [arXiv:1602.03837 [gr-qc]] [Search INSPIRE].
- [2] B. P. Abbott *et al.* (LIGO Scientific and Virgo Collaborations), Properties of the Binary Black Hole Merger GW150914, *Phys. Rev. Lett.* **116**, 241102 (2016) [arXiv:1602.03840 [gr-qc]] [Search INSPIRE].
- [3] B. P. Abbott *et al.* Multi-messenger Observations of a Binary Neutron Star Merger, *Astrophys. J.* **848**, L12 (2017) [arXiv:1710.05833 [astro-ph.HE]] [Search INSPIRE].
- [4] B. P. Abbott *et al.* (LIGO Scientific and Virgo Collaborations), GWTC-1: A Gravitational-Wave Transient Catalog of Compact Binary Mergers Observed by LIGO and Virgo during the First and Second Observing Runs, [arXiv:1811.12907 [astro-ph.HE]] [Search INSPIRE].
- [5] H. Weyl, The theory of gravitation, *Ann. Phys. (N.Y.)* **54**, 117 (1917) [Search INSPIRE].
- [6] S. D. Majumdar, A class of exact solutions of Einstein’s field equations, *Phys. Rev.* **72**, 390 (1947) [Search INSPIRE].
- [7] A. Papapetrou, A static solution of the equations of the gravitational field for an arbitrary charge distribution, *Proc. R. Ir. Acad., Sect. A* **51**, 191 (1947) [Search INSPIRE].
- [8] J. B. Hartle and S. W. Hawking, Solutions of the Einstein–Maxwell equations with many black holes, *Commun. Math. Phys.* **26**, 87 (1972) [Search INSPIRE].
- [9] D. Kramer and G. Neugebauer, The superposition of two Kerr solutions, *Phys. Lett. A*, **75**, 259 (1980).
- [10] D. Nitta, T. Chiba, and N. Sugiyama, Shadows of Colliding Black Holes, *Phys. Rev. D* **84**, 063008 (2011) [arXiv:1106.2425 [gr-qc]] [Search INSPIRE].
- [11] A. Bohn, W. Thrope, F. Hébert, K. Henriksson, D. Bunandar, M. A. Scheel, and N. W. Taylor, What does a binary black hole merger look like?, *Class. Quant. Grav.* **32**, 065002 (2015) [arXiv:1410.7775 [gr-qc]] [Search INSPIRE].
- [12] M. Patil, P. Mishra, and D. Narasimha, Curious case of gravitational lensing by binary black holes: a tale of two photon spheres, new relativistic images and caustics, *Phys. Rev. D* **95**, 024026 (2017) [arXiv:1610.04863 [gr-qc]] [Search INSPIRE].
- [13] T. Assumcao, V. Cardoso, A. Ishibashi, M. Richartz, and M. Zilhao, Black hole binaries: ergoregions, photon surfaces, wave scattering, and quasinormal modes, *Phys. Rev. D* **98**, 064036 (2018) [arXiv:1806.07909 [gr-qc]] [Search INSPIRE].
- [14] P. V. P. Cunha, C. A. R. Herdeiro, and M. J. Rodriguez, Shadows of Exact Binary Black Holes, *Phys. Rev. D* **98**, 044053 (2018) [arXiv:1805.03798 [gr-qc]] [Search INSPIRE].
- [15] M. Campanelli, M. Dettwyler, M. Hannam, and C. O. Lousto, Relativistic three-body effects in black hole coalescence, *Phys. Rev. D* **74**, 087503 (2006) [arXiv:astro-ph/0509814] [Search INSPIRE].
- [16] Y. Torigoe, K. Hattori, and H. Asada, Gravitational waveforms for 2 and 3-body gravitating systems, *Phys. Rev. Lett.* **102**, 251101 (2009) [arXiv:0906.1448 [gr-qc]] [Search INSPIRE].

- [17] N. Seto, Relativistic Resonant Relations between Massive Black Hole Binary and Extreme Mass Ratio Inspiral, *Phys. Rev. D* **85**, 064037 (2012) [arXiv:1202.4761 [astro-ph.CO]] [Search INSPIRE].
- [18] K. Yamada and H. Asada, Nonchaotic evolution of triangular configuration due to gravitational radiation reaction in the three-body problem, *Phys. Rev. D* **93**, 084027 (2016) [arXiv:1512.01087 [gr-qc]] [Search INSPIRE].
- [19] K. Hayasaki, S. Mineshige, and H. Sudou, Binary Black Hole Accretion Flows in Merged Galactic Nuclei, *Publ. Astron. Soc. Jpn.* **59**, 427 (2007) [astro-ph/0609144] [Search INSPIRE].
- [20] H. Kimitake, S. Mineshige, and L. C. Ho, A supermassive binary black hole with triple disks, *Astrophys. J.* **682**, 1134 (2008) [arXiv:0708.2555 [astro-ph]] [Search INSPIRE].
- [21] I. D. Novikov and K. S. Thorne, Astrophysics of black holes, in *Black Holes (Les Astres Occus)*, edited by C. DeWitte and B. DeWitt (Gordon and Breach, New York, 1973), p. 343.
- [22] J. P. A. Clark and D. M. Eardley, Evolution of close neutron star binaries, *Astrophys. J.* **215**, 311 (1977).
- [23] L. E. Kidder, C. M. Will, and A. G. Wiseman, Coalescing binary systems of compact objects to (post)^{5/2}-Newtonian order. III. Transition from inspiral to plunge, *Phys. Rev. D* **47**, 3281 (1993) [Search INSPIRE].
- [24] A. Wunsch, T. Muller, D. Weiskopf, and G. Wunner, Circular orbits in the extreme Reissner–Nordström dihole metric, *Phys. Rev. D* **87**, 024007 (2013) [arXiv:1301.7560 [gr-qc]] [Search INSPIRE].
- [25] S. R. Dolan and J. O. Shipley, Stable photon orbits in stationary axisymmetric electrovacuum spacetimes, *Phys. Rev. D* **94**, 044038 (2016) [arXiv:1605.07193 [gr-qc]] [Search INSPIRE].
- [26] T. Igata, H. Ishihara, and Y. Takamori, Stable Bound Orbits around Black Rings, *Phys. Rev. D* **82**, 101501 (2010) [arXiv:1006.3129 [hep-th]] [Search INSPIRE].
- [27] T. Igata, H. Ishihara, and H. Yoshino, Integrability of Particle System around a Ring Source as the Newtonian Limit of a Black Ring, *Phys. Rev. D* **91**, 084042 (2015) [arXiv:1412.7033 [hep-th]] [Search INSPIRE].
- [28] J. Camps, S. Hadar, and N. S. Manton, Exact Gravitational Wave Signatures from Colliding Extreme Black Holes, *Phys. Rev. D* **96**, 061501 (2017) [arXiv:1704.08520 [gr-qc]] [Search INSPIRE].
- [29] P. Jai-akson, A. Chatrabhuti, O. Evnin, and L. Lehner, Black hole merger estimates in Einstein–Maxwell and Einstein–Maxwell–dilaton gravity, *Phys. Rev. D* **96**, 044031 (2017) [arXiv:1706.06519 [gr-qc]] [Search INSPIRE].
- [30] J. Shipley and S. R. Dolan, Binary black hole shadows, chaotic scattering and the Cantor set, *Class. Quant. Grav.* **33**, 175001 (2016) [arXiv:1603.04469 [gr-qc]] [Search INSPIRE].

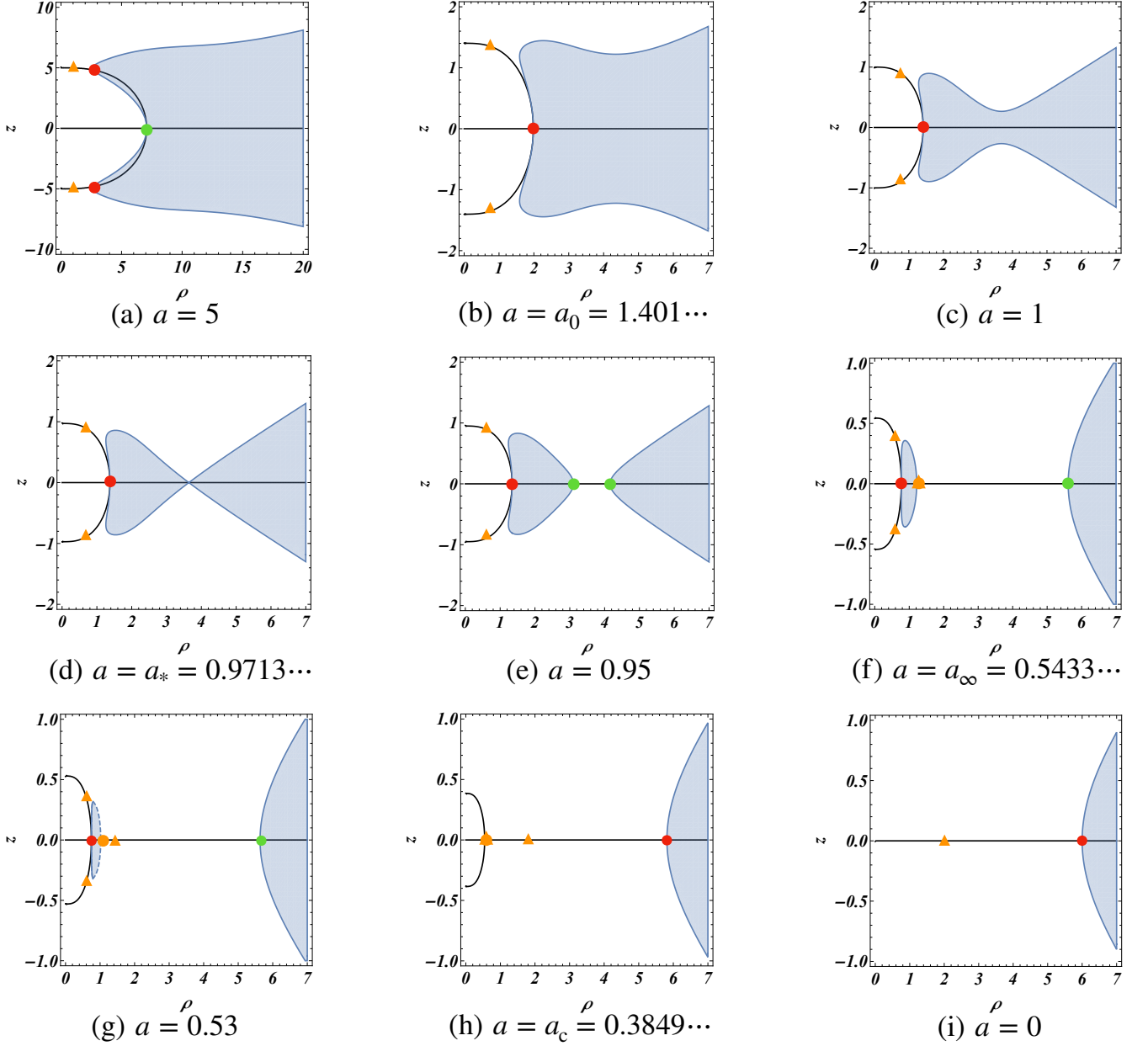


FIG. 1: Positions of stable circular orbits of massive particles in ρ - z plane of the Majumdar–Papapetrou dihole spacetime with equal mass $M_+ = M_- = 1$ for the separation range $0 \leq a \leq 5$. The solid black lines represent the curves satisfying $U_z = 0$ (i.e., $z = 0$ and $\rho = \rho_0$). The shaded regions show the region D , where $h_0 > 0$, $k_0 > 0$, and $L_0^2 > 0$ are satisfied. The sequence of stable circular orbits is the solid black curves included in the region D . The solid blue lines are the boundary of D where $h_0 = 0$, $L_0^2 > 0$, and $k_0 > 0$. The dashed blue lines are the boundary of D where $h_0 > 0$, $k_0 > 0$, and L_0^2 diverges. The red dots are the positions of ISCOs. The green dots are the positions of marginally stable circular orbits (MSCOs) except for the ISCO. The orange triangles and dots are the positions of unstable circular photon orbits and stable ones, where L_0^2 diverges. (a) $a = 5$: When a is large enough, stable circular orbits exist not only on $z = 0$ line in the range $\rho \in (\sqrt{2}a, \infty)$ but on $\rho = \rho_0$ line. An MSCO exists at $(\rho, z) = (\sqrt{2}a, 0)$, and the ISCOs are located around each black hole. (b) $a = a_0 = 1.401\dots$: There exist stable circular orbits on $z = 0$ plane in the range $\rho \in (\sqrt{2}a_0, \infty)$. The ISCO is located at $(\rho, z) = (\sqrt{2}a_0, 0)$, where three MSCOs for $a > a_0$ are degenerate. (c) $a = 1$: There exist stable circular orbits on $z = 0$ plane in the range $\rho \in (\sqrt{2}, \infty)$. The point $(\rho, z) = (\sqrt{2}, 0)$ is the ISCO. (d) $a = a_* = 0.9713\dots$: The region D is marginally connected at $(\rho, z) = (\rho_*, 0)$. There exist stable circular orbits on $z = 0$ plane in the range $\rho \in (\sqrt{2}a_*, \infty)$, of which the boundary $(\rho, z) = (\sqrt{2}a_*, 0)$ is the ISCO. (e) $a = 0.95$: The sequence of stable circular orbits splits into two parts. As a result, two additional MSCOs appear at the boundary of the outer sequence and the outer boundary of the inner sequence. The point $(\rho, z) = (\sqrt{2}a, 0)$ is the ISCO. (f) $a = a_\infty = 0.5433\dots$: There are two sequences of stable circular orbits. The outer boundary of the inner sequence is no longer physical because L_0^2 diverges there. An MSCO appears at the boundary of the outer sequence, and the ISCO appears at $(\rho, z) = (\sqrt{2}a_\infty, 0)$. (g) $a = 0.53$: There are two sequences of stable circular orbits. At the outer boundary of the inner sequence, L_0^2 diverges. An MSCO appears at the boundary of the outer sequence, and the ISCO appears at $(\rho, z) = (\sqrt{2}a, 0)$. (h) $a = a_c = 0.3849\dots$: The divergence of L_0^2 occurs at $(\rho, z) = (\sqrt{2}a_c, 0)$ and the inner sequence of stable circular orbits disappears. There only exists the outer sequence and its inner boundary becomes the ISCO. (i) $a = 0$: There exist stable circular orbits in the range $\rho \in (6, \infty)$ on $z = 0$. The point $(\rho, z) = (6, 0)$ is the ISCO, which connects to the ISCO of the single extremal Reissner–Nordström black hole with mass 2.

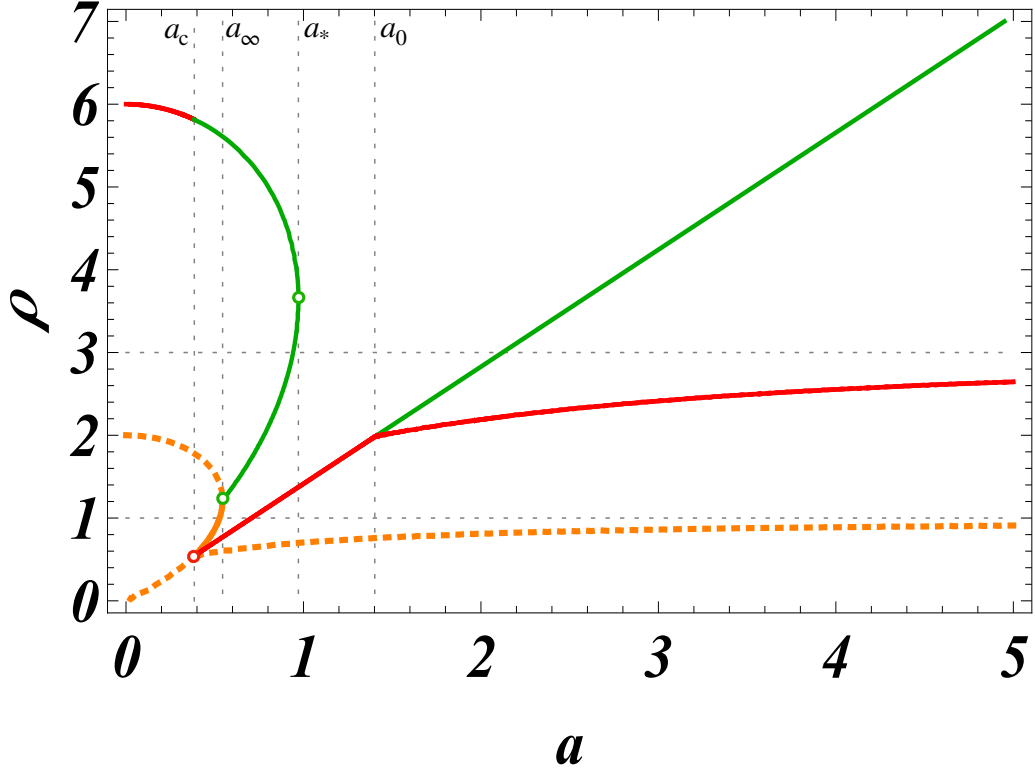


FIG. 2: Dependence of the radii of marginally stable circular orbits and circular photon orbits on the separation parameter a in the Majumdar–Papapetrou dihole spacetime with equal unit mass. The red and green solid lines mark the radii of the marginally stable circular orbits (MSCOs) and innermost stable circular orbits (ISCOs), respectively. The orange dashed lines and the orange solid line are the unstable circular photon orbits and the stable circular photon orbits, respectively. For $a_c < a \leq a_\infty$, the radius of the ISCO is smaller than that of the stable circular photon orbit. At $a = a_c$, a discontinuous transition of ISCO occurs.